

Backscattering enhancement from polariton-polariton coupling on a rough metal surface

K. A. O'Donnell and C. S. West

The School of Physics, Georgia Institute of Technology, Atlanta, Georgia 30332

E. R. Méndez

Division de Física Aplicada, Centro de Investigación Científica y de Educación Superior de Ensenada, Ensenada, Baja California, Mexico

(Received 14 November 1997; revised manuscript received 19 February 1998)

We consider the angular dependence of the light diffusely scattered from a silver surface with weak one-dimensional roughness. The power spectrum of the random roughness is significant at twice the surface plasmon polariton wave number. At high incidence angles, an enhanced backscattering peak is experimentally observed in the mean diffuse intensity. This peak does not occur in perturbation theory that is exact to fourth order in the surface profile. From a sixth-order perturbation term that expresses an intensity contribution arising from the coupling of counterpropagating plasmon polaritons, we obtain a backscattering peak that is closely consistent with the observations. It is demonstrated that this sixth-order backscattering effect exhibits behavior that is significantly different from a fourth-order effect occurring for other roughness spectra. [S0163-1829(98)02720-9]

I. INTRODUCTION

Backscattering enhancement of light scattered from randomly rough surfaces has attracted interest in recent years. The effect is seen, in the mean diffusely scattered intensity, as a distinct peak in the direction of retroreflection. For a bare metal surface, two types of the effect appear. In the case of a steeply sloped surface with root mean square (rms) roughness σ comparable to the illumination wavelength λ , multiple scattering within surface valleys has been found to produce a backscattering peak.^{1,2} On the other hand, another type of backscattering enhancement relies on the excitation of surface plasmon polaritons; it occurs for finely scaled surfaces with $\sigma \ll \lambda$.^{3,4} Even though the scattering mechanisms are quite different, both backscattering effects arise from the constructive interference of multiple scattering processes. Indeed, analogous scattering processes are responsible for the backscattering peaks noted in the light scattered from collections of small particles,⁵ as well as for the weak localization of electron waves in random solids.⁶

Since the earliest works appeared, the polariton-related surface backscattering effect has seen a sustained level of interest. There have been further related studies of the angular dependence of the diffuse scatter that employ perturbation theory^{7,8} or numerical simulations.⁹ It is quite recently that experimental observations of this backscattering effect were first reported,^{10,11} the delay is due largely to the difficulties encountered in the fabrication of rough surfaces producing adequate polariton coupling. These observations were followed by favorable comparisons with perturbation theory,¹² as well as calculations that suggested experimental extensions.¹³ Other theoretical works have addressed the angular correlation functions of the scattered light,¹⁴ where more subtle consequences of the constructive interference are apparent. Further, a theoretical study of diffuse second-harmonic generation from rough metal surfaces has considered the effects of plasmon-polariton excitation at the funda-

mental and harmonic frequencies;¹⁵ peaks were predicted both at backscattering and in a direction normal to the average surface. Despite what appeared to be rapid experimental confirmations,¹⁶ later works have claimed that the first peak is instead a deep minimum^{17,18} and that the second does not exist.¹⁹

In this paper, we provide an experimental and theoretical study of polariton-related backscattering enhancement. Our purpose is to demonstrate that there are two types of this effect that may arise distinctly from one another. In the first, light-polariton coupling is fully responsible for the effect and there is no need to consider polariton-polariton scattering. This is the nature of the previous experimental observations,^{10,11} where polariton-polariton coupling is forbidden by the power spectrum of the surface roughness. These observations thus agree closely with perturbation calculations in (σ/λ) that are exact to only fourth order,¹² an order that includes light-polariton coupling but neglects polariton-polariton coupling. A second example that is approximately of this type is presented in Fig. 2(a) of Ref. 3; the scattering distribution was shown to be reasonably consistent with fourth-order theory in a later work.⁸

Our main efforts here are made to introduce the second type of the effect, in which the backscattering peak arises solely from polariton-polariton coupling. In particular, an essential step in the formation of the peak is that a plasmon polariton must be roughness coupled to a counterpropagating plasmon polariton. The total isolation of this polariton-polariton process arises in a natural way from our surface roughness spectrum. The effect is clearly observable in the experiments but the surface structure must be unusually finely scaled and, under the conditions employed here, the angle of incidence must be large.

The paper is organized as follows. In Sec. II, we first describe experimental observations of this backscattering effect with a well-characterized surface having highly one-dimensional roughness. The experiment is conducted in the

infrared with a roughness power spectrum of a displaced rectangular form. The measured diffuse intensities are there briefly compared with perturbation theory that is exact to fourth order in the parameter (σ/λ). Even though the parameter is small ($\sigma/\lambda \cong 10^{-2}$), the polariton-polariton coupling is neglected and the backscattering effect is absent.

After pointing out the limitations of this theory in Sec. III, in Sec. IV we present the theoretical development necessary to produce the effect. A perturbation term of sixth order that expresses the polariton-polariton scattering processes is developed and evaluated without approximation. Excellent comparisons are made with the experimental predictions, and additional calculations based on numerical solution of Green's integral theorem also support the results. Further, a relation is pointed out between the effect considered here and certain aspects of earlier theoretical calculations. Approximate forms of our results are obtained in Sec. V, where properties of the backscattering effect considered here are shown to be different from the fourth-order effect.

II. EXPERIMENTAL RESULTS

In the experimental work described here, we employ a surface having a power spectrum of a displaced rectangular form. This spectrum is related to that developed for the observations of the fourth-order backscattering effect,^{10,11} here the effect may be observed as long as the plasmon-polariton wave number falls within the nonzero part of the rectangular spectrum.¹¹ It will be seen in Sec. V that the high-order backscattering effect requires a spectrum that is significant at twice the plasmon polariton wave number. We stress that the rectangular spectrum remains an experimental necessity for us; the broad Gaussian spectra common in theoretical works⁷⁻⁹ are far beyond our fabrication capabilities.

The surface was made using extensions of holographic grating fabrication techniques.¹⁰ Briefly, a 50×50 -mm glass plate was coated with a $1.5\text{-}\mu\text{m}$ layer of Shipley S1400-27 photoresist. The plate was exposed to $N=500$ sinusoidal intensity distributions arising at the intersection of two light beams. The source was a HeCd laser of wavelength 442 nm. Each sinusoidal pattern had a different spatial wave number k in the direction along the plate and was randomly phased with respect to all other exposures. The minimum and maximum exposure wave numbers ($k_{\min}=9.93 \times 10^{-3} \text{ nm}^{-1}$ and $k_{\max}=1.49 \times 10^{-2} \text{ nm}^{-1}$, respectively) were well-known from the exposing geometry. With the exposure wave numbers evenly spaced between k_{\min} and k_{\max} , the net exposure behaves as a Fourier series that, in the limit of large N , becomes consistent with a Gaussian random process.¹⁰ The plate was then developed in a manner producing a linear relation between exposure and resulting surface height (30 sec in Shipley 352 developer). The surface roughness obtained was highly one-dimensional as is assumed in our later calculations.

After a thick layer (400 nm) of silver was evaporated onto the sample at a pressure less than 10^{-6} Torr, it was characterized with a Talystep stylus profilometer. The power spectrum $\mathcal{G}(k)$ of the surface roughness was computed from the profilometer data and is shown in Fig. 1. The measured spectrum rises significantly between k_{\min} and k_{\max} and is near the rectangular form desired. The rms roughness σ is 11.1 nm.

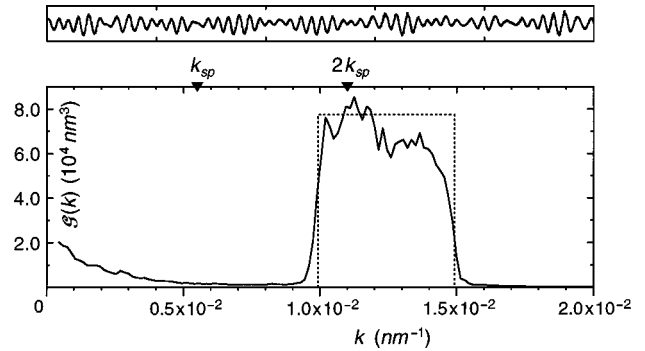


FIG. 1. Top: Segment of a typical profilometer scan of the surface. The vertical scale is ± 30 nm and horizontal axis ticks are spaced by 5000 nm. Bottom: For positive k , the measured power spectrum $\mathcal{G}(k)$ of the surface roughness (solid curve), compared with the idealized $\mathcal{G}(k)$ used in calculations (dashed rectangle). Normalization is such that $2\pi\sigma^2$ is $\int_{-\infty}^{\infty} \mathcal{G}(k) dk$.

This sample has been employed elsewhere for other purposes.¹⁷

The scattering instrument is of simple principle similar to that described elsewhere.^{10,11} The source was a Jodon HN-20 HeNe laser of wavelength $\lambda = 1152$ nm. The slightly convergent incident beam was p polarized (electric field in the plane of incidence) and had diameter 4 mm at the sample. The sample was mounted on a rotation stage to set the incidence angle θ_i . A detector arm mounted on a concentric motorized rotation stage produced scans in scattering angle θ_s along the plane of incidence. The detector was a cooled InSb detector whose signal was processed by an Ithaco 3981 lock-in amplifier. In front of the detector, a slit 60 cm from the surface determined the detector integration angle to be of 0.4° full width. To reduce speckle noise, the sample was translated over the uniformly rough surface area (25 mm width) as the detector signal was averaged to provide each data point. Further, results are expressed as a normalized diffuse intensity $I_p(\theta_s)$ that represents the mean diffusely scattered power per radian for unit incident power. The specular reflection was of narrow width and is not shown in the diffuse data presented here.

The experimental results are shown in Fig. 2. For modest θ_i , the surface produces little diffuse scatter. This is true from normal incidence to $\theta_i = 50^\circ$, which is the smallest incidence angle shown in Fig. 2. For $\theta_i = 56^\circ$, $I_p(\theta_s)$ has increased for both $\theta_s < -54^\circ$ and $\theta_s > 54^\circ$, and a distinct peak is seen at backscattering ($\theta_s = -\theta_i$). For $\theta_i = 58^\circ$, 60° , and 62° , this peak persists there, with height comparable to that of the surrounding distribution. The distribution is seen to rise rapidly for negative θ_s near grazing (this increase is seen, for example, for $\theta_s < -70^\circ$ with $\theta_i = 62^\circ$). We find that the backscattering peak is difficult to discern when it falls near the steep slope in $I_p(\theta_s)$ (which occurs for $62^\circ < \theta_i < 70^\circ$), but the peak can again be seen for $\theta_i = 70^\circ$ and 76° as shown in Fig. 2. In these latter two cases it appears in the midst of high levels of $I_p(\theta_s)$, but the absolute height of the peak above the surrounding scattering levels has not changed greatly upon comparison with results for smaller θ_i . Surprisingly, as θ_i increases in Fig. 2, the diffusely scattered power continues to rise from 0.0041 ($\theta_i = 50^\circ$) to 0.023 ($\theta_i = 58^\circ$), 0.031 ($\theta_i = 62^\circ$), and 0.070 ($\theta_i = 76^\circ$).

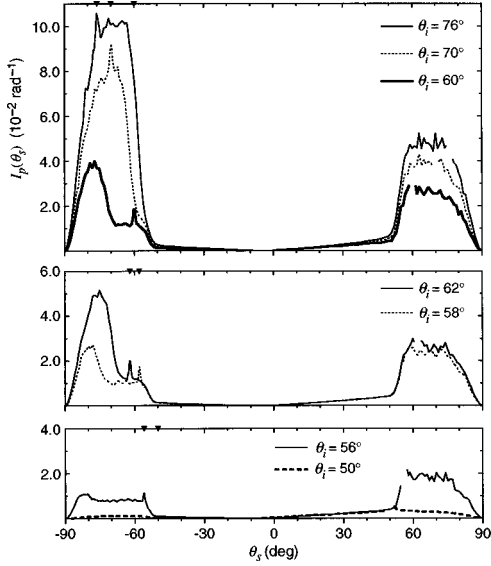


FIG. 2. Measurements of the mean diffuse intensity $I_p(\theta_s)$ for wavelength 1152 nm, p polarization, and incidence angles θ_i as shown. A peak persists at backscattering (note the inverted triangles) for all cases except $\theta_i = 50^\circ$.

In order to make some initial comparisons with these data, we have evaluated the perturbation theory of Ref. 8 for $I_p(\theta_s)$, which is exact to fourth order in (σ/λ) . In these calculations, the roughness spectrum $\mathcal{G}(k)$ was assumed to have an ideal rectangular form for $\sigma = 11.1$ nm (see Fig. 1), all integrals were evaluated numerically without approximation, and we have assumed the dielectric constant to be $\epsilon = -61.0 + 6.2i$. This value of ϵ was obtained by slightly increasing the imaginary part of a published value,²⁰ so as to provide agreement with the experimental height of $I_p(\theta_s)$ for $\theta_s > 54^\circ$. The results are shown in Fig. 3 for $\theta_i = 62^\circ$ and 76° . There is some agreement between theory and experiment; for $\theta_s > 54^\circ$ the perturbation theory closely reproduces the shape of the experimental distribution. Further, in the case for $\theta_i = 62^\circ$, at $\theta_s \cong -70^\circ$ the perturbation theory reproduces well the steep slope of the experimental $I_p(\theta_s)$ followed by its more gradual fall toward $\theta_s = -90^\circ$. However, the experimental scatter falling for $-70^\circ < \theta_s < -54^\circ$, which includes the backscattering peak, is completely absent in this calculation. In the second case with $\theta_i = 76^\circ$, the high distribution for negative θ_s is generally similar to the experimental result and diffuse scatter now appears at backscattering, but the backscattering peak is again absent.

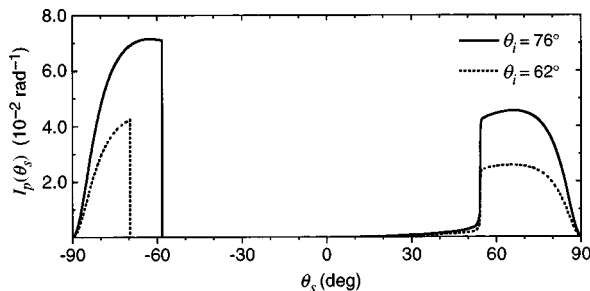


FIG. 3. For the incidence angles θ_i shown, the mean diffuse intensity $I_p(\theta_s)$ calculated from the perturbation theory that is exact to fourth order.

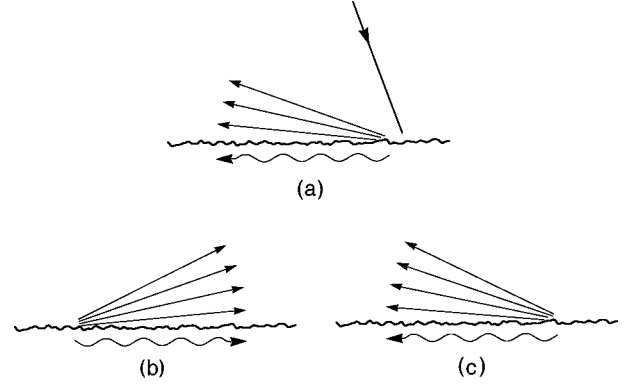


FIG. 4. The sequence of scattering events occurring on the rough metal surface. In (a), the incident wave produces diffuse scatter and an initial excitation of $-k_{sp}$. Then, in (b), $-k_{sp}$ is scattered to produce diffuse light and an excitation of $+k_{sp}$. Finally, $+k_{sp}$ is scattered to produce diffuse light and an excitation of $-k_{sp}$ in (c).

We have tried using more accurate models of the experimental spectrum in the calculations. For example, including the low levels of $\mathcal{G}(k)$ seen in Fig. 1 for small k produces low levels of scatter for $0^\circ < \theta_s < 50^\circ$ in a manner more consistent with the experimental results, and accounting for the modest linear trend seen between k_{\min} and k_{\max} in Fig. 1 does change the height of the results of Fig. 3 slightly. However, these modifications are minor. It is thus clear that this perturbation theory, although fully capable of predicting backscattering effects with other surface spectra, predicts no such effect in the case discussed here.

III. DISCUSSION

In order to resolve this situation, we consider the scattering processes occurring on this rough surface. We start with the processes that are included in the perturbation theory of Sec. II, and then discuss what processes are missing in that theory.

The arguments made consider the sequence of scattering events shown in Fig. 4. First, in Fig. 4(a), the incident wave strikes the surface and is scattered by the roughness. In lowest-order perturbation theory, the diffuse scatter emerges from the surface at scattering angles θ_s satisfying the coupling equation

$$q = k + k_r, \quad (1)$$

where $k = (\omega/c)\sin\theta_i$ is the component of the incident wave vector parallel to the mean surface, $q = (\omega/c)\sin\theta_s$ is an analogous quantity for a propagating scattered wave, ω is the frequency, and k_r is a roughness wave number where the spectrum $\mathcal{G}(k_r)$ is significant. We term this process single scatter.

As shown in Fig. 1, we idealize $\mathcal{G}(k_r)$ as being of constant height and nonzero only within the limits of $[-k_{\max}, -k_{\min}]$ and $[k_{\min}, k_{\max}]$. One may then compute the scattering angle coupling ranges that follow from Eq. (1). The positive wave numbers of $\mathcal{G}(k_r)$ produce only evanescent scatter (i.e., $|q| > \omega/c$) but the negative wave numbers of $\mathcal{G}(k_r)$ produce scatter to negative θ_s from $q = k - k_{\min}$ out to grazing ($q = k - k_{\max}$ remains evanescent). These ranges are $-90^\circ < \theta_s < -70^\circ$ for $\theta_i = 62^\circ$ and $-90^\circ < \theta_s < -58^\circ$ for $\theta_i = 76^\circ$. In

Fig. 3, the theory produces single-scattering distributions of leading order $(\sigma/\lambda)^2$ within these ranges.

However, this type of coupling may also lead to the excitation of plasmon polaritons. This excitation will occur if q in Eq. (1) coincides with a plasmon polariton as in

$$\pm k_{sp} = k + k_r, \quad (2)$$

where $\pm k_{sp} = \pm(\omega/c)\sqrt{\varepsilon_r/(\varepsilon_r+1)}$ is the wave number of the plasmon polariton traveling to the right (+) or left (-), $\varepsilon = \varepsilon_r + i\varepsilon_i$ is the dielectric constant, and we find $k_{sp} \cong 1.01(\omega/c)$ for the value of ε cited earlier. It is readily verified that, for the idealized $\mathcal{G}(k_r)$, Eq. (2) is consistent with the excitation of $-k_{sp}$, but $+k_{sp}$ is not excited because there is no appropriate wave number present in $\mathcal{G}(k_r)$.

The excited surface wave $-k_{sp}$ may significantly affect the scattering distribution as it is scattered by the surface roughness, producing the waves of Fig. 4(b). This scattering process would again be described by Eq. (2), but with k being replaced by $-k_{sp}$ as in

$$q = -k_{sp} + k'_r, \quad (3)$$

where k'_r is a second wave number available in $\mathcal{G}(k'_r)$. We find that only the positive-wave-number part of $\mathcal{G}(k'_r)$ produces propagating scatter in Eq. (3). This coupling range may be readily calculated from the properties of $\mathcal{G}(k'_r)$ and appears at $54^\circ < \theta_s < 90^\circ$ in Fig. 3. In the self-consistent theory, the mechanism just discussed produces a distribution there of order $(\sigma/\lambda)^4$. We term this process double scattering, as the net coupling requires both k_r and k'_r .

We now consider the processes missing in the perturbation theory of Ref. 8. First, we note that the coupling of the previous paragraph may lead to excitation of $+k_{sp}$. This follows if we replace q by $+k_{sp}$ in Eq. (3) as

$$+k_{sp} = -k_{sp} + k'_r. \quad (4)$$

The roughness wave number required is $k'_r = 2k_{sp}$, which is clearly present in $\mathcal{G}(k'_r)$ in Fig. 1. The excited surface wave $+k_{sp}$ may now give rise to diffuse scatter, producing the waves of Fig. 4(c). The coupling equation follows analogously to Eq. (3) as

$$q = +k_{sp} + k''_r, \quad (5)$$

where k''_r is an appropriate roughness wave number. Equation (5) predicts that the negative-wave-number part of $\mathcal{G}(k''_r)$ is consistent with diffuse scatter directed to $-90^\circ < \theta_s < -54^\circ$. We term this process triple scattering and it is expected to arise in a perturbation term of order $(\sigma/\lambda)^6$.

The experimental results of Fig. 2 show a distribution lying within this angular range. Because the backscattering peak is seen within this distribution, in Sec. IV we seek a sixth-order perturbation term as the origin of the backscattering effect. We also note that, because $\mathcal{G}(\pm 2k_{sp}) > 0$, the roughness will produce yet further couplings of $+k_{sp}$ to $-k_{sp}$ and vice versa, of increasing order in (σ/λ) . However, these processes become less and less significant, particularly when it is realized that the next plasmon-related contribution to this backscattering peak would require two more roughness couplings and hence would appear in the tenth order. Here, we evaluate only the sixth-order term.

IV. THEORY

A complete description of the perturbation approach based on the reduced Rayleigh equations may be found in Ref. 8. Equations that follow directly from Ref. 8 will thus be presented here with little justification, but the evaluation of the relevant term has not appeared elsewhere and will be described in more detail. As in Sec. II, all scattering distributions computed throughout Secs. IV–V assume that $\varepsilon = -61.0 + 6.2i$, $\sigma = 11.1$ nm, $\lambda = 1152$ nm, and that $\mathcal{G}(k)$ has the ideal rectangular form of Fig. 1.

We assume that the one-dimensional surface roughness is consistent with a Gaussian process. In this case only even powers of (σ/λ) appear in the perturbation series for $I_p(\theta_s)$; the sixth is the next nonvanishing order. The exact sixth-order contribution to $I_p(\theta_s)$ follows from Ref. 8 as

$$\begin{aligned} I_p^{(6)}(\theta_s) = & \frac{1}{L_1} \frac{2}{\pi} \left(\frac{\omega}{c}\right)^3 \cos^2 \theta_s \cos \theta_i |G_0(q)|^2 |G_0(k)|^2 \\ & \times \left\{ \frac{1}{36} \langle |T^{(3)}(q|k)|^2 \rangle - \frac{1}{24} \text{Re}[\langle T^{(2)*}(q|k)T^{(4)} \right. \\ & \times (q|k) \rangle - \langle T^{(2)*}(q|k) \rangle \langle T^{(4)}(q|k) \rangle] \\ & \left. + \frac{1}{60} \text{Re} \langle T^{(1)*}(q|k)T^{(5)}(q|k) \rangle \right\}, \quad (6) \end{aligned}$$

where $T^{(n)}(q|k)$ is the transition matrix perturbation term of order n in the surface profile, L_1 is the length of the illuminated surface in the direction along the one-dimensional roughness, and the angle brackets denote an ensemble average. $G_0(k)$ is the plasmon polariton Green's function for a flat metal surface,

$$G_0(k) = \frac{i\varepsilon}{\varepsilon\alpha_0(k) + \alpha(k)}, \quad (7)$$

where $\alpha_0(k) = \sqrt{(\omega/c)^2 - k^2}$ and $\alpha(k) = \sqrt{\varepsilon(\omega/c)^2 - k^2}$. As stated in Sec. III, we seek effects arising from scattering processes involving three surface wave numbers. Such processes are present only in the term of Eq. (6) having $T^{(3)}(q|k)$. The term involving $T^{(1)*}(q|k)T^{(5)}(q|k)$ may be shown to be a sixth-order correction to the single-scattering distribution. Similarly, the term having $T^{(2)*}(q|k)T^{(4)}(q|k)$ may be considered a correction to the double-scattering distribution. Hence we restrict our efforts to an exact evaluation of only $\langle |T^{(3)}(q|k)|^2 \rangle$ and, although we thus neglect other terms of order $(\sigma/\lambda)^6$, we do collect all contributions arising from the scattering mechanism of interest.

The quantity $T^{(3)}(q|k)$ is developed in Ref. 8 as

$$\begin{aligned} T^{(3)}(q|k) = & V^{(3)}(q|k) + 3 \int_{-\infty}^{\infty} \frac{dp}{2\pi} V^{(2)}(q|p)G_0(p)V^{(1)}(p|k) \\ & + 3 \int_{-\infty}^{\infty} \frac{dp}{2\pi} V^{(1)}(q|p)G_0(p)V^{(2)}(p|k) \\ & + 6 \int_{-\infty}^{\infty} \frac{dp}{2\pi} \int_{-\infty}^{\infty} \frac{dr}{2\pi} V^{(1)}(q|p)G_0(p)V^{(1)} \\ & \times (p|r)G_0(r)V^{(1)}(r|k), \quad (8) \end{aligned}$$

where $V^{(n)}(q|k)$ is the perturbation term of the scattering potential of n th order in the surface profile. In particular, we have

$$V^{(1)}(q|k) = i \frac{\varepsilon - 1}{\varepsilon^2} [\varepsilon q k - \alpha(q)\alpha(k)] \hat{\zeta}(q-k), \quad (9)$$

where $\hat{\zeta}(k)$ is the Fourier transform of the surface profile function $\zeta(x)$ as in

$$\hat{\zeta}(k) = \int_{-\infty}^{\infty} dx \zeta(x) \exp(-ikx). \quad (10)$$

The quantities $V^{(2)}(q|k)$ and $V^{(3)}(q|k)$ are more lengthy but are given explicitly in Ref. 8. For our purposes it is most useful to write Eq. (8) in a different form. By inserting the expressions for the $V^{(n)}(q|k)$, it is possible to cast Eq. (8) as

$$T^{(3)}(q|k) = \int \int_{-\infty}^{\infty} \frac{dp}{2\pi} \frac{dr}{2\pi} \times \mathcal{A}(q|p|r|k) \hat{\zeta}(q-p) \hat{\zeta}(p-r) \hat{\zeta}(r-k), \quad (11)$$

where $\mathcal{A}(q|p|r|k)$ is given by

$$\begin{aligned} \mathcal{A}(q|p|r|k) = & \frac{3i(\varepsilon-1)^2}{2\varepsilon^3} \{(p^2+r^2)[\varepsilon q k - \alpha(q)\alpha(k)] - 2[pk - \alpha(k)^2]\alpha(q)\alpha(p)\} + \frac{i(\varepsilon-1)}{\varepsilon^3} \alpha(q)\alpha(k) \left\{ \frac{3}{2}(\varepsilon-1)(q^2+k^2) \right. \\ & - 2\varepsilon\alpha(q)\alpha(k) + (\varepsilon-2)[\alpha(q)^2 + \alpha(k)^2] \} + \frac{i(\varepsilon-1)}{\varepsilon^3} qk \{ 2\alpha(q)\alpha(k) - \frac{1}{2}\varepsilon(\varepsilon-1)(q^2+k^2) \\ & + \varepsilon[\alpha(q)^2 + \alpha(k)^2] \} - \frac{3i(\varepsilon-1)^2}{\varepsilon^3} \alpha(r)\alpha(k) [qr - \alpha(q)^2] - \frac{6i(\varepsilon-1)^3}{\varepsilon^4} \alpha(q)\alpha(p)\alpha(r)\alpha(k) \\ & - \frac{3(\varepsilon-1)^2}{\varepsilon^4} [\varepsilon rk - \alpha(r)\alpha(k)] G_0(r) \times \left\{ \frac{2(\varepsilon-1)}{\varepsilon} \alpha(q)\alpha(p)\alpha(r) + [\alpha(q) + \alpha(r)][qr - \alpha(q)\alpha(r)] \right\} \\ & - \frac{3(\varepsilon-1)^2}{\varepsilon^4} [\varepsilon qp - \alpha(q)\alpha(p)] G_0(p) \times \left\{ \frac{2(\varepsilon-1)}{\varepsilon} \alpha(p)\alpha(r)\alpha(k) + [\alpha(p) + \alpha(k)][pk - \alpha(p)\alpha(k)] \right. \\ & \left. + \frac{2i(\varepsilon-1)}{\varepsilon^2} [\varepsilon pr - \alpha(p)\alpha(r)] G_0(r) [\varepsilon rk - \alpha(r)\alpha(k)] \right\}. \end{aligned} \quad (12)$$

A typographical error in line 3 of Eq. (3.24c) of Ref. 8 has been corrected in Eq. (12) above. By squaring and averaging Eq. (11), it follows directly that

$$\begin{aligned} \langle |T^{(3)}(q|k)|^2 \rangle = & \int \int \int \int_{-\infty}^{\infty} \frac{dp}{(2\pi)^4} \frac{dr}{(2\pi)^4} \frac{dp'}{(2\pi)^4} \frac{dr'}{(2\pi)^4} \\ & \times \mathcal{A}(q|p|r|k) \mathcal{A}^*(q|p'|r'|k) \\ & \times \langle \hat{\zeta}(q-p) \hat{\zeta}(p-r) \hat{\zeta}(r-k) \\ & \times \hat{\zeta}^*(q-p') \hat{\zeta}^*(p'-r') \hat{\zeta}^*(r'-k) \rangle. \end{aligned} \quad (13)$$

The moment within the integral may be evaluated by substituting Eq. (10) for the six Fourier transforms and applying the Gaussian moment theorem to $\zeta(x)$. This produces 15 terms, each of which contains δ functions. After carrying out

the trivial integrations in a manner analogous to that of Ref. 8, we obtain the expression

$$\begin{aligned} \langle |T^{(3)}(q|k)|^2 \rangle = & \frac{\sigma^6}{(2\pi)^2} L_1 \left\{ \int \int_{-\infty}^{\infty} \mathcal{A}(q|p|r|k) \mathcal{S}^*(q,p,r,k) \right. \\ & \times g(q-p)g(p-r)g(r-k) dp dr \\ & + g(q-k) \left| \int_{-\infty}^{\infty} \mathcal{A}(q|p|q|k) g(q-p) dp \right. \\ & + \int_{-\infty}^{\infty} \mathcal{A}(q|k|r|k) g(r-k) dr \\ & \left. + \int_{-\infty}^{\infty} \mathcal{A}(q|p|k-q+p|k) g(q-p) dp \right|^2, \end{aligned} \quad (14)$$

where $\mathcal{S}(q,p,r,k)$ is given by

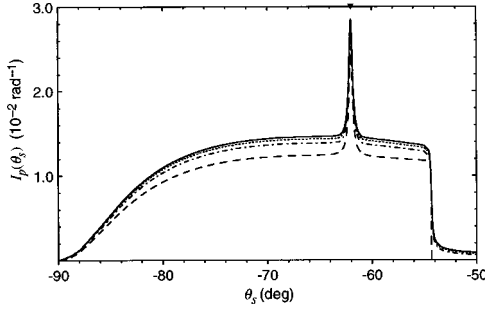


FIG. 5. The intensity contribution $\mathcal{I}(\theta_s)$ for $\theta_i = 62^\circ$. Results are obtained from exact integration (solid curve), the approximation of Eq. (17) (finely-dashed curve, just below solid curve), the approximations of both Eqs. (17) and (19) (dot-dashed curve), and the pole approximation of Sec. V (coarsely dashed curve).

$$\begin{aligned} \mathcal{S}(q,p,r,k) = & \mathcal{A}(q|p|r|k) + \mathcal{A}(q|p|k+p-r|k) + \mathcal{A}(q|q-p \\ & + r|r|k) + \mathcal{A}(q|q+k-r|k+p-r|k) \\ & + \mathcal{A}(q|q-p+r|q+k-p|k) \\ & + \mathcal{A}(q|q+k-r|q+k-p|k), \end{aligned} \quad (15)$$

and $\sigma^2 g(k) = \mathcal{G}(k)$. Equations (14) and (15) thus represent our general result for the term of interest.

We have evaluated the integrals of Eq. (14) exactly using numerical quadrature, employing the parameters of Sec. II to allow comparisons with the experiment. First, we note that the term that is the squared modulus of three integrals in Eq. (14) contributes only in the region of single scatter because of the common factor $g(q-k)$. The associated scattering contribution is found to be at most a few percent of the height of the single-scatter distributions of Fig. 3 and, although we include it in later results, this contribution is of secondary interest. Instead, the double integral of Eq. (14) is far more significant; from Eq. (6) it produces a diffuse intensity contribution $\mathcal{I}(\theta_s)$ of

$$\begin{aligned} \mathcal{I}(\theta_s) = & \frac{\sigma^6}{72\pi^3} \left(\frac{\omega}{c}\right)^3 \cos^2 \theta_s \cos \theta_i |G_0(q)|^2 |G_0(k)|^2 \\ & \times \int \int_{-\infty}^{\infty} \mathcal{A}(q|p|r|k) \mathcal{S}^*(q,p,r,k) \\ & \times g(q-p)g(p-r)g(r-k) dp dr. \end{aligned} \quad (16)$$

We show numerical results for $\mathcal{I}(\theta_s)$ in Fig. 5 for $\theta_i = 62^\circ$, where a distribution rises for $-90^\circ < \theta_s < -54^\circ$. This range is indeed that expected for the outward roughness coupling of $+k_{sp}$ to diffuse scatter, as was discussed in Sec. III. Further, a distinct peak appears at backscattering, having a height above the background exactly equal to the height of the surrounding distribution.

We briefly consider two simplifications of this theory. First, in Eq. (8) for $T^{(3)}(q|k)$, we consider the effect of ignoring all term contributions having $V^{(2)}$ and $V^{(3)}$, but keeping the one involving only $V^{(1)}$. From Eqs. (8), (9), and (11), it is clear that $\mathcal{A}(q|p|r|k)$ is thus simplified to the form

$$\mathcal{A}(q|p|r|k) = 6u(q|p)G_0(p)u(p|r)G_0(r)u(r|k), \quad (17)$$

where

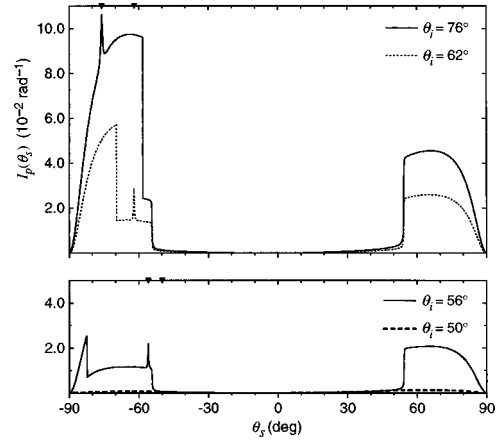


FIG. 6. For the incidence angles θ_i shown, the diffuse intensity $I_p(\theta_s)$ obtained by adding the intensity contribution from exact evaluation of $\langle |T^{(3)}(q|k)|^2 \rangle$ to the results of the fourth-order self-consistent theory.

$$u(q|k) = i \frac{\varepsilon - 1}{\varepsilon^2} [\varepsilon qk - \alpha(q)\alpha(k)]. \quad (18)$$

Results for $\mathcal{I}(\theta_s)$ using Eq. (17) are shown in Fig. 5 and are only slightly below the exact calculations. The approximate calculations are considerably faster and thus can be useful if this level of numerical accuracy is adequate.

Further, for either form of $\mathcal{A}(q|p|r|k)$, we find that the first and last terms of $\mathcal{S}(q,p,r,k)$ in Eq. (15) are far more significant than the other four terms. This suggests the approximation

$$\mathcal{S}(q,p,r,k) = \mathcal{A}(q|p|r|k) + \mathcal{A}(q|q+k-r|q+k-p|k). \quad (19)$$

Calculations of $\mathcal{I}(\theta_s)$ using both approximations of Eqs. (17) and (19) are also shown in Fig. 5, where the results are lower still than those of the first simplification, but the agreement with the exact evaluations remains good. The broad distribution of Fig. 5 arises largely from integration of the first term of Eq. (19), while only the second term produces the backscattering peak.

We now return to the exact calculations and evaluate Eq. (14) with the complete versions of $\mathcal{A}(q|p|r|k)$ and $\mathcal{S}(q,p,r,k)$. The contribution to the diffuse intensity from only $\langle |T^{(3)}(q|k)|^2 \rangle$ is found from Eq. (6) and is added to the fourth-order self-consistent intensity of Sec. II. The total intensity thus includes all perturbation terms of second and fourth order in (σ/λ) , as well as the sixth-order term chosen to include processes of interest. These results are shown in Fig. 6 and are to be compared directly with the data of Fig. 2. For $\theta_i = 50^\circ$ there is no initial excitation of $-k_{sp}$, the single-scatter contribution is evanescent, and a low distribution appears in the calculation that is similar to the experimental results. At $\theta_i = 56^\circ, 62^\circ$, and 76° , the consequences of $\pm k_{sp}$ excitation are seen for $|\theta_s| > 54^\circ$. In the former two cases the backscattering peak occurs in isolated sixth-order scatter and, in the latter case, it appears in the midst of high single-scattering contributions. The agreement with the experimental data remains excellent throughout the results.

To further support our results we now briefly compare with rigorous calculations using an integral equation

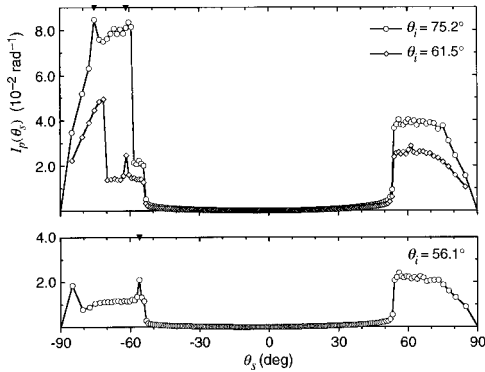


FIG. 7. Normalized mean diffuse intensity $I_p(\theta_s)$ calculated by a rigorous numerical simulation in which a periodic rough surface is illuminated by a plane wave. The results correspond to an average over 2250 surface realizations. The points shown represent the mean diffuse intensity due to the Bragg orders of the periodic surface.

formalism.² Applying Green's integral theorem to the regions above and below the interface, two coupled integral equations are established. The solution of these equations determines the source functions that are required for the calculation of the scattered field. Usually, the use of tapered beam illumination^{2,21} permits the truncation of the infinite surface to a finite interval, without introducing significant distortion of the scattering distribution due to edge effects. In the present case, however, the excitation of surface polaritons plays a prominent role in the resulting scattering curves. Even for the longest surfaces that can be studied with computers available to us, the scattering results we obtain are length dependent because the surface length is comparable to the plasmon polariton decay length. One way of avoiding this problem is by imposing a periodicity to the surface profile, so that an infinite sample can be considered. The solution to this problem can be obtained in the usual manner, with the added cost of evaluating the periodic Green's functions and their normal derivatives on the surface. The efficient evaluation of these functions is critical for the feasibility of the method, and we use rapidly converging integral forms for this purpose.²²

Thus, we in fact calculate the scattering of light from a classical grating, albeit one with a long period and a Gaussian random profile within that period, illuminated by a plane wave. The scattering problem is then reduced to solving a matrix equation for the amplitudes of the Bragg waves diffracted by each realization of the grating. The estimate of the mean intensity is obtained by averaging over an ensemble of statistically identical surfaces. The total diffuse intensity is thus obtained directly without regard to the perturbation order of the scattering contributions. The sampling interval on the surface was chosen as $\lambda/12$ and a total of 1024 points per period were used. It is also convenient to choose the incident angles in such a way that the matrix does not have to be recalculated for each angle. For this reason, the θ_i chosen are close but not identical to those of Fig. 6. The calculated points in the scattering distributions appear at the positions of the grating orders and, for our choice of θ_i , there is always a point in the backscattering direction.

These results are shown in Fig. 7 for $\theta_i = 56.1^\circ$, 61.5° , and 75.2° . All cases contain backscattering peaks, although

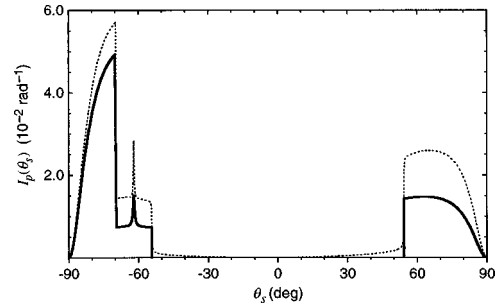


FIG. 8. The mean diffuse intensity $I_p(\theta_s)$ from Ref. 3 for $\theta_i = 62^\circ$ (solid curve). Also shown is the comparable result from Fig. 6 (dashed curve).

the angular structure of the peaks is not well resolved in this method, particularly for larger θ_i . It is quite impressive that, for all θ_s where isolated contributions from $\langle |T^{(3)}(q|k)|^2 \rangle$ appear in Fig. 6 (even in the ledge at $\theta_s \cong -57^\circ$ for $\theta_i = 76^\circ$), the results of Fig. 7 are in excellent agreement with the perturbation theory. Additionally, for $\theta_i = 56.1^\circ$ and 61.5° , the scatter for $\theta_s > 54^\circ$ in Fig. 7 is in close agreement with the perturbation results, although the perturbation theory is slightly higher there for $\theta_i = 75.2^\circ$. Modest differences are also to be seen in the regions having single-scatter contributions, again particularly for $\theta_i = 75.2^\circ$. We speculate that the latter differences could arise from the neglected 1–5 term in Eq. (6), while the first difference could arise from the neglected 2–4 term. Nonetheless, the agreement between Figs. 7 and 6 is satisfying.

Finally, we note that high-order processes were included in the two theoretical works that originally predicted backscattering enhancement for a slightly rough surface,^{3,4} later work⁷ has also followed suit in estimating the effects of high-order coupling. Reference 3 is appropriate for the case here and, to compare with our other calculations, we have evaluated the expressions for our rectangular spectrum. The results are shown in Fig. 8 for $\theta_i = 62^\circ$. The general appearance of the resulting distribution is similar to our calculations and, most impressively, a distinct peak indeed appears at backscattering. The theory does contain fourth-order terms that produce much of the backscattering effect of Ref. 3 but, appropriately, these terms play no role in the backscattering effect in Fig. 8. Instead this peak arises, as it should, from yet higher-order terms.

This theory was applied in Refs. 2 and 3 to the case of a wide Gaussian spectrum, centered on zero wave number, for which backscattering enhancement would appear in terms of fourth and higher orders. The intent of including the higher-order terms was largely to provide height and width corrections to the backscattering peak; it was not recognized that the sixth-order effect could be isolated as it has been here. Hence the terms were approximated because it was impractical to make the theory self-consistent in each order. It was only some years later that the exact fourth-order term was first developed,⁸ and the sixth-order term of Eq. (6) still has not been fully evaluated.

Indeed, it can be seen that the heights of the plasmon-related scattering contributions in Fig. 8 are approximately half of the levels of Fig. 6. However, the theory is being used here in a manner far from its original intent and we do not criticize it. References 3 and 4 are admirable for pointing out

that, for the Gaussian spectrum, a backscattering peak would appear in the fourth order, and that higher-order terms contain other coherent processes that contribute to the shape of the peak. Our work considers one of these processes in the sixth order, well isolated through the use of the rectangular spectrum.

V. DISCUSSION

By examining the perturbation theory, we now consider in more detail the physical mechanisms that give rise to the backscattering effect. It was discussed in Sec. IV that excellent approximate results were obtained by keeping the term having only $V^{(1)}$ in the expression for $T^{(3)}(q|k)$. From Eq. (8) we approximately have

$$T^{(3)}(q|k) = 6 \int_{-\infty}^{\infty} \frac{dp}{2\pi} \int_{-\infty}^{\infty} \frac{dr}{2\pi} V^{(1)}(q|p) G_0(p) V^{(1)}(p|r) G_0(r) V^{(1)}(r|k). \quad (20)$$

By reading the quantities within the integral from right to left, this scattering process is readily interpreted. The potential $V^{(1)}(r|k)$ represents the scatter of the incident wave k by the roughness, with its transformation into a plasmon polariton $r = -k_{sp}$. This wave then travels along the surface [$G_0(r)$] and is scattered to the state $p = +k_{sp}$ by a second scattering event $V^{(1)}(p|r)$. As described by the Green's function $G_0(p)$, this wave propagates along the surface, until it is converted to an outgoing wave q through a final scattering event $V^{(1)}(q|p)$.

Direct evidence of this scattering process may be found through approximate evaluation of the results of Sec. IV. We substitute the approximations of Eqs. (17) and (19) into the sixth-order intensity $\mathcal{I}(\theta_s)$ of Eq. (16). The resulting integrand contains products of Green's functions that may be treated with pole approximations.⁸ For example, within the pole approximation,

$$|G_0(p)|^2 \cong \frac{\pi C^2}{\Delta_\varepsilon} [\delta(p - k_{sp}) + \delta(p + k_{sp})] \quad (21)$$

and

$$G_0(p) G_0^*(x-p) \cong \frac{2\pi i C^2}{2i\Delta_\varepsilon - x} \delta(p - k_{sp}) + \frac{2\pi i C^2}{2i\Delta_\varepsilon + x} \delta(p + k_{sp}), \quad (22)$$

where

$$C = \frac{|\varepsilon_r|^{3/2}}{\varepsilon_r^2 - 1} \quad (23)$$

and

$$\Delta_\varepsilon = \frac{1}{2} \varepsilon_i \frac{k_{sp}}{|\varepsilon_r| [|\varepsilon_r| - 1]}. \quad (24)$$

Upon carrying out the integrations over δ functions we obtain eight terms. However, four of them contain $g(0)$ and are thus zero for the idealized spectrum of Fig. 1. Two more

terms may be dropped because there is no direct coupling of the incident wave to $+k_{sp}$ [a factor $g(k_{sp} - k)$ thus vanishes]. We then obtain

$$\begin{aligned} \mathcal{I}(\theta_s) = & \frac{\sigma^6}{2\pi^3} \left(\frac{\omega}{c}\right)^3 \cos^2 \theta_s \cos \theta_i |G_0(q)|^2 |G_0(k)|^2 \\ & \times g(q - k_{sp}) g(2k_{sp}) g(-k_{sp} - k) \\ & \times \left\{ \left(\frac{\pi C^2}{\Delta_\varepsilon}\right)^2 |u(q|k_{sp})|^2 |u(k_{sp} - k_{sp})|^2 \right. \\ & \times |u(-k_{sp}|k)|^2 + \frac{(\pi C^2)^2}{\Delta_\varepsilon^2 + [(q+k)/2]^2} |u(q|k_{sp})|^2 \\ & \left. \times |u(k_{sp} - k_{sp})|^2 |u(-k_{sp}|k)|^2 \right\}. \quad (25) \end{aligned}$$

In the second term within the curly brackets we have set $q = -k$ when it appeared in the arguments of the functions $u()$, with an excellent approximation; the term's dependence on q and k is instead dominated by the narrow Lorentzian factor. By reading the arguments of the $u()$ from right to left in Eq. (25), the wave-number sequence $k \rightarrow -k_{sp} \rightarrow +k_{sp} \rightarrow q$ is apparent that is consistent with our earlier discussions. The two terms within the curly brackets of Eq. (25) become identical at backscattering, with the second term producing a peak there of Lorentzian form. The full width at half maximum of the peak follows from the Lorentzian factor as $\Delta q = 4\Delta_\varepsilon$ or, in scattering angle θ_s , as $\Delta\theta_s = 4c\Delta_\varepsilon/(\omega \cos \theta_i)$. Equation (25) also makes clear that, although the effect appears only at high angles for the surface considered here, this is not essential. In principle, this backscattering effect could appear for any θ_i , as long as $g(k)$ is of adequate height at the points required by Eq. (25).

The pole approximation is readily evaluated and is compared with earlier results in Fig. 5. It predicts a distribution slightly lower than that obtained by exact evaluation of the same integrand, but the comparison with the other results is still good. The peak width $\Delta\theta_s$ is 0.42° in both the pole approximation results and in the exact calculations, in agreement with the expression given above for $\Delta\theta_s$. The results obtained with the pole approximation hence contain all essential features seen in the exact calculations.

We claim that, as is the case for other forms of backscattering enhancement, the distinct peak seen throughout our results arises from the constructive interference of multiple scattering contributions. Consider the situation shown in Fig. 9(a). An incident wave strikes the point x_1 of the rough surface and launches the surface wave $-k_{sp}$. This wave is scattered at point x_2 into $+k_{sp}$, which travels until it finally is scattered a third time, being converted to a propagating wave at point x_3 . For every such path shown, there is a time-reversed path in which the same scattering events occur, but in a reversed order as $x_3 \rightarrow x_2 \rightarrow x_1$. The scattering contributions from these two paths are phase coherent at backscattering and interfere perfectly constructively there, but they interfere with a random phase relationship far from backscattering. After averaging, the first term in the curly brackets of Eq. (25) represents the total intensity arising

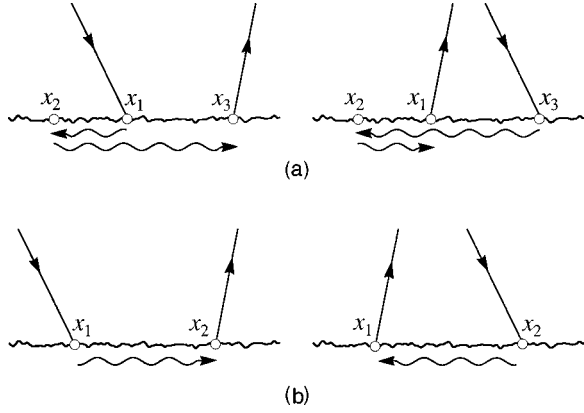


FIG. 9. Pairs of scattering processes related by time reversal for the sixth-order effect (a) and fourth-order effect (b); lines below the rough surface indicate plasmon polariton coupling.

ing from all such paths, and the second term represents the interference between pairs of paths related by time-reversal symmetry.

We have demonstrated here that this backscattering effect may be readily observed when the backscattering effect of order $(\sigma/\lambda)^4$ is absent. It would thus seem reasonable to consider the two effects as being distinct from one another. We can provide additional, albeit subtle, evidence of this assertion by consideration of the physical mechanism producing the fourth-order effect.⁸ Here, as shown in Fig. 9(b), an incident wave is scattered from point x_1 and is converted into the plasmon polariton $+k_{sp}$. It is then scattered from a point x_2 to escape as a propagating wave. In the time-reversed path, it is the counterpropagating polariton $-k_{sp}$ that travels from x_2 to x_1 . In this effect, the enhancement thus arises from the interference of the distinct processes $k \rightarrow +k_{sp} \rightarrow q$ and $k \rightarrow -k_{sp} \rightarrow q$. However, both of these couplings are forbidden at backscattering by the spectrum of our surface, so the fourth-order effect is absent. As discussed earlier, in the sixth-order effect there is only the single process $k \rightarrow -k_{sp} \rightarrow +k_{sp} \rightarrow q$. That is, the sixth-order effect differs in that the forward and time-reversed paths of Fig. 9(a) use an identical wave-number scattering sequence.

This observation has the mathematical consequence that, in the pole approximation, the sixth-order effect described here is simpler than the fourth-order effect. The intensity contribution of Eq. (25) is composed of only two terms. However, the pole approximation for the fourth-order effect [see Eq. (5.9) of Ref. 8] necessarily yields four terms, with the interference between the two sequences clearly seen in the two terms of the enhancement peak. No such interference is noted in the single term of Eq. (25) for the sixth-order peak.

More significantly, these differences have physical consequences. It has been demonstrated that the diffuse scattering contributions from the forward and time-reversed paths of Fig. 9(b) may be physically separated for the fourth-order effect, in a manner described elsewhere.¹¹ However, we claim that no analogous separation can be observed for the sixth-order effect because Eq. (25) describes a single indivisible wave-number sequence.

To provide a simple illustration of this point we consider the quasiperiodic metal surface,

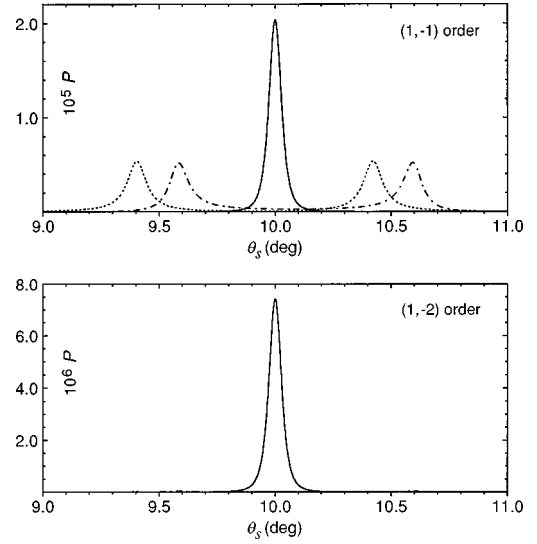


FIG. 10. Top: From fourth-order theory, the dimensionless power P of the $(1,-1)$ diffracted order from a quasiperiodic surface with $k_1 = 0.004552 \text{ nm}^{-1}$ and $k_2 = 0.006446 \text{ nm}^{-1}$. Bottom: From sixth-order theory, P for the $(1,-2)$ order with $k_1 = 0.01100 \text{ nm}^{-1}$ and k_2 unchanged. In both cases $A_1 = 1 \text{ nm}$, $A_2 = 1 \text{ nm}$, and simultaneous plasmon-polariton coupling occurs for $\lambda = 1152 \text{ nm}$ (solid line). Detuned cases have $\lambda = 1142 \text{ nm}$ (dashed curve) and $\lambda = 1162 \text{ nm}$ (dot-dashed curve); these cases are too small to be seen in the lower plot. For all λ , we assume $\epsilon = -61.0 + 6.2i$.

$$\zeta(x) = A_1 \sin(k_1 x) + A_2 \sin(k_2 x + \phi), \quad (26)$$

where all quantities are deterministic. An experimental study of the fourth-order scatter for this type of surface²³ has revealed the two scattering processes of Fig. 9(b), because such a surface allows simultaneous excitation of $+k_{sp}$ (through, say, wave number k_1) as well as $-k_{sp}$ (through k_2). The scattered light then escapes from the surface in a diffracted order that satisfies

$$\frac{\omega}{c} \sin \theta_s = \frac{\omega}{c} \sin \theta_i + n k_1 + m k_2 \quad (27)$$

with $(n, m) = (1, -1)$. We assume, somewhat arbitrarily, that the simultaneous plasmon excitation occurs for $\theta_i = 10^\circ$, which determines the values of k_1 and k_2 . Using the complete fourth-order perturbation theory, we compute the power of the $(1,-1)$ order as shown in Fig. 10(a). The high peak occurs as the order passes through backscattering and contains contributions from both processes of Fig. 9(b). The two processes may now be seen as distinct from one another by simply tuning the source wavelength, as is apparent in the two peaks for other λ in Fig. 10(a). In particular, the separate peaks indicate that the distinct processes of Fig. 9 do indeed still occur, but they do not occur simultaneously. The height of the main peak of Fig. 10(a) is almost exactly four times that of the detuned cases, which indicates perfectly constructive interference.

To consider the analogous sixth order effect, we change only k_1 to $2k_{sp}$ so as to provide the coupling of counterpropagating plasmon polaritons. The triple-scattering process of Fig. 9(a) involves three roughness wave numbers and is thus found in the order $(n, m) = (1, -2)$ in Eq. (27). Using

the complete sixth-order perturbation theory, we compute the power in this order as shown in Fig. 10(b). As was the case in Fig. 10(a), a single peak appears due to the triple-scattering process as the order passes through backscattering. However, as the source is detuned the peak disappears and little trace of scattering contributions remains. This technique hence cannot separate the effect into two distinct contributions of equal amplitude.

Figure 10 thus simply illustrates an essential difference between the two scattering processes. Related effects occur for rough surfaces; in a manner analogous to Fig. 10(a), tuning the source in the fourth-order effect can produce a clear angular separation of the two diffuse scattering contributions arising via the forward and time-reversed paths of Fig. 9.¹¹ A similar tuning experiment with the pure sixth-order effect would have quite different consequences, without such separation. As the source is tuned for our rectangular spectrum, Eq. (25) indicates that the *entire* distribution $\mathcal{I}(\theta_s)$ would, as a whole, shift in angle because of the factor $g(q - k_{sp})g(-k_{sp} - k)$. Further, the factor $g(2k_{sp})$ indicates that the distribution would simply vanish if the tuning were so large that $g(2k_{sp}) = 0$.

VI. CONCLUSIONS

The work described here began with the unexpected experimental observation of a backscattering peak in the light diffusely scattered from a slightly rough silver surface. The experiments made use of a well-characterized surface and scattering data were taken under fully controlled conditions. It was clear that the observed effect was not present in the theoretical prediction for the diffuse intensity exact to fourth

order in the parameter (σ/λ) . In an evaluation of a sixth-order perturbation term, the effect was found to arise from triple-scattering contributions related to the excitation of surface plasmon polaritons. Excellent agreement with the controlled experimental data was obtained. Further comparisons were made with approximate evaluations of the perturbation term, computer simulations based on Green's integral theorem, and with a previous perturbation approach that included terms of sixth and higher order.

There are a number of notable properties of the sixth-order backscattering effect as it has been described here. Although the surface roughness is weak ($\sigma/\lambda \cong 10^{-2}$), lowest-order perturbation theory is inadequate and contributions of even sixth order in σ/λ play an essential role. In addition, this type of backscattering effect has been observed here at unusually large incidence angles as high as 76° . Our restriction to large θ_i is a consequence of the roughness spectrum employed here, but the same effect could also occur at small θ_i for other surface spectra. Finally, it is remarkable that it is possible to isolate the scattering contributions of second, fourth, and sixth order in (σ/λ) , thus making obvious their relative significance.

If our use of a roughness spectrum of a displaced rectangular form may seem contrived, we point out that the scattering processes discussed here would occur to some extent for a sufficiently wide spectrum having, for example, a Gaussian form centered on zero wave number. However, the scattering distribution of the less contrived surface would be far more difficult to interpret, with the various scattering processes overlapping in angle. Even though the displaced rectangular spectrum remains an experimental necessity for us, the distinct scattering contributions associated with it also have been essential to the main conclusions of this paper.

¹K. A. O'Donnell and E. R. Méndez, *J. Opt. Soc. Am. A* **4**, 1194 (1987).

²A. A. Maradudin, T. Michel, A. R. McGurn, and E. R. Méndez, *Ann. Phys. (N.Y.)* **203**, 255 (1990).

³A. R. McGurn, A. A. Maradudin, and V. Celli, *Phys. Rev. B* **31**, 4866 (1985).

⁴V. Celli, A. A. Maradudin, A. M. Marvin, and A. R. McGurn, *J. Opt. Soc. Am. A* **2**, 2225 (1985).

⁵Y. Kuga and A. Ishimaru, *J. Opt. Soc. Am. A* **1**, 831 (1984); M. P. van Albada and A. Lagendijk, *Phys. Rev. Lett.* **55**, 2692 (1985); P. E. Wolf and G. Maret, *ibid.* **55**, 2696 (1985); D. S. Wiersma, P. Bartolini, A. Lagendijk, and R. Righini, *Nature (London)* **390**, 671 (1997).

⁶P. Sheng, *Introduction to Wave Scattering, Localization, and Mesoscopic Phenomena* (Academic, San Diego, 1995).

⁷A. R. McGurn and A. A. Maradudin, *J. Opt. Soc. Am. B* **4**, 910 (1987); V. Freilikher and I. Yurkevich, *Phys. Lett. A* **183**, 247 (1993); **183**, 253 (1993); H. Ogura and Z. L. Wang, *Phys. Rev. B* **53**, 10 358 (1996); M. Arnold and A. Otto, *Opt. Commun.* **125**, 122 (1996); H. Hanato, H. Ogura, and Z. L. Wang, *Waves Random Media* **7**, 11 (1997).

⁸A. A. Maradudin and E. R. Méndez, *Appl. Opt.* **32**, 3335 (1993).

⁹P. Tran and V. Celli, *J. Opt. Soc. Am. A* **5**, 1635 (1988); T. R. Michel, *ibid.* **11**, 1874 (1994).

¹⁰C. S. West and K. A. O'Donnell, *J. Opt. Soc. Am. A* **12**, 390 (1995).

¹¹C. S. West and K. A. O'Donnell, *Opt. Lett.* **21**, 1 (1996).

¹²A. A. Maradudin, A. R. McGurn, and E. R. Méndez, *J. Opt. Soc. Am. A* **12**, 2500 (1995).

¹³A. R. McGurn and A. A. Maradudin, *Waves Random Media* **6**, 251 (1996).

¹⁴A. Arsenieva and S. Feng, *Phys. Rev. B* **47**, 13 047 (1993); V. Malyshkin, A. R. McGurn, T. A. Leskova, A. A. Maradudin, and M. Nieto-Vesperinas, *Waves Random Media* **7**, 479 (1997); *Opt. Lett.* **22**, 946 (1997).

¹⁵A. R. McGurn, T. A. Leskova, and V. M. Agranovich, *Phys. Rev. B* **44**, 11 441 (1991).

¹⁶X. Wang and H. J. Simon, *Opt. Lett.* **16**, 1475 (1991); H. J. Simon, Y. Wang, L. Zhou, and Z. Chen, *ibid.* **16**, 1268 (1992); O. A. Aktsipetrov, V. N. Golovkina, O. I. Kapusta, T. A. Leskova, and N. N. Novikova, *Phys. Lett. A* **170**, 231 (1992); Y. Wang and H. J. Simon, *Phys. Rev. B* **47**, 13 695 (1993).

¹⁷K. A. O'Donnell, R. Torre, and C. S. West, *Opt. Lett.* **21**, 1738 (1996).

¹⁸M. Leyva-Lucero, E. R. Méndez, T. A. Leskova, A. A. Maradudin, and J. Q. Lu, *Opt. Lett.* **21**, 1809 (1996).

¹⁹K. A. O'Donnell, R. Torre, and C. S. West, *Phys. Rev. B* **55**, 7985 (1997).

²⁰D. W. Lynch and W. R. Hunter, in *Handbook of Optical Constants of Solids*, edited by Edward D. Palik (Academic, New York, 1985), p. 356.

²¹E. I. Thorsos, *J. Acoust. Soc. Am.* **83**, 78 (1988).

²²M. E. Veysoglu, H. A. Yuch, R. T. Shin, and J. A. Kong, *J. Electromagn. Waves Appl.* **5**, 267 (1991).

²³C. S. West and K. A. O'Donnell, *Opt. Commun.* **123**, 109 (1996).